2024 IEEE/RSJ International Conference on Intelligent Robots and Systems (IROS)
October 14-18, 2024. Abu Dhabi, UAE

A parallel-actuated robot with two end-effector degrees-of-freedom: Application as a novel wearable head-neck traction brace

Jingzong Zhou, Priya Kulkarni, and Sunil Agrawal

Abstract— **This paper describes a parallel-actuated robotic mechanism designed to provide two degrees-of-freedom (DOF) to the end-effector relative to a fixed base. In a potential application as a head-neck traction brace, these two independent DOFs are the vertical translation of the head with respect to shoulders and a specified orientation of the head in lateral bending. Motivated by recommended clinical methods to apply traction forces on the head, it is designed to provide vertical traction force on the head while tilted in a specific orientation. The design has four chains starting from a base stationed at the shoulders, each chain having 5 DOFs. Each chain imposes a single constraint on the motion of the end-effector. Together, four chains would apply four constraints, allowing only two DOFs of motion to the end-effector. Two out of four component chains are actively driven by linear actuators. Our kinematic studies show that the achievable workspace of this mechanism with a specific stroke length of actuators of $\pm$ 50 mm results in 175-222 mm of vertical translation and up to $\pm$ 9 $^\circ$ of lateral bending. The lateral bending is coupled to the flexion/extension angle of the end-effector. A physical prototype was constructed to investigate the functional realization of the design in hardware. Overall, the physical prototype validated the motion of the theoretical model despite potential errors in the fabrication, making the design a candidate for potential head-neck traction application.**

I. INTRODUCTION

Radiological findings indicate that 90% of men above 50 years and 90% of women above 60 years show degenerative changes in the cervical spine [1]. This degeneration in the cervical spine is known as cervical spondylosis, which includes deterioration of intervertebral discs, hypertrophy of facets, and ligamentous and segmental instability [2]. These changes result in irritation and compression of the nerve roots leading to loss of fine motor functions in the upper limbs and pain in the neck [3], [4]. Cervical spondylosis is a common condition among the elderly and accounts for nearly 2% of all hospital admissions in the United States [1].

Surgical procedures such as an anterior cervical discectomy and fusion can be used to treat cervical spondylosis and the resulting disability it can cause [5]. Furthermore, improvement in cervical spondylosis from surgical intervention is observed but the ideal surgical approach remains debatable. Complications of surgical intervention include wound infection and muscular motor weakness [6]. To avoid the risks associated with surgical intervention, clinicians may opt for a more conservative treatment by applying a traction force on the head [7]. Traction refers to the application of a decompressing force on the spine and is a common treatment to relieve the symptoms of cervical radiculopathy [7].

In a clinical setting, manual traction is used where a clinician holds the patient's head in the hand and manipulates it while applying the force [7]. In a case series, it has been reported that 91% of patients treated with manual physical therapy of the neck exhibit reduced pain at the time of discharge and at 6-month follow-up [8].

Traction may also be applied using a mechanical system, which allows for the application of intermittent traction. In a reported study [9], 15 patients with different levels of cervical radiculopathy were treated with mechanical intermittent cervical traction. The outcome showed that patients with radicular symptoms lasting 12 weeks or less demonstrated a reduction in pain after the treatment [9]. Another study with 123 participants showed that the application of upper cervical traction improved active cervical rotation and pain response. The study suggests that mechanical traction force, with lateral bending, can improve cervical rotation range of motion and reduce neck pain [10]. Another study indicates that the range of motion for axial rotation, flexion/extension and lateral bending is significantly improved through cervical traction and exercise therapy [11].

Current treatment methods for cervical traction have several limitations: (i) lack of control of the head posture relative to the shoulders when traction force is applied, (ii) poor control of the traction force over time, and (iii) inability to perform other functions when participants lie on a bench and undergo traction.

The limitations of current cervical traction methods may be remedied through the use of robotic neck braces. An existing soft wearable device with four pneumatic actuators to actively assist upper extremity movements has proved success in reaching tasks [12]. Additionally, an active neck brace with three rotational degrees-of-freedom (DOFs) was designed to help patients with head drop by our group at Columbia University [13] [14] [15]. While these braces allow natural motion of the head relative to the shoulders, the vertical translation of the head is coupled to the rotation of the head. A recent design was proposed in [16] to actively control the position of the head. However, this mechanism does not verify the device's ability to perform independent vertical translation. Another group also used a 3 RPS structure with the aim of alleviating pain in the neck [17]. However, in their design the vertical motion is coupled to the rotation and the research only focused on flexion/extension and lateral bending [17]. A 6-DOF spatial parallel mechanism, consisting of a 6-3 UPS Stewart

Authors are all from Mechanical Engineering Department of Columbia University in the city of New York, Email: {jz3293, pk2689, sa3077}@columbia.edu

platform, was analyzed as a candidate for a rehabilitation device for patients with neck pain, however, traction was not explored as an application [18].

Currently, robotic neck braces lack the ability to provide an independent z-translation motion while also being able to position the head in lateral bending and flexion. This capability is fundamental to traction applications where traction force will be applied along the vertical direction while the orientation of the neck can be adjusted using the rotational DOFs. Therefore, a new device must be proposed which can achieve these goals.

The neck brace proposed in this paper has a completely new and different architecture compared to every head-neck brace design proposed in the literature. Our proposed design allows 2 DOF at the end-effector and uses a 4-chain parallel mechanism. The architecture of this neck brace has been specifically chosen to provide vertical translation to the head relative to the shoulders while the neck is in a specific orientation. The detailed kinematics of this special 2-DOF design has not been studied in the literature. It is important to point out that the design of this 4-chain parallel mechanism was conceptualized by our research team as an extension to a 3-chain parallel mechanism structure proposed in [19]. The kinematics of this 3-chain parallel mechanism was not formally analyzed in the literature or fabricated in hardware. Our group showed the feasibility of this design in hardware and demonstrated both position and force control for it [20].

The proposed mechanism's two controllable DOFs are the vertical translation and lateral bending angle. With this choice of the mechanism, the vertical translation DOF would be used to control the traction force and the lateral bending would be used to select the head orientation of the patient with cervical spondylosis [10]. In this paper, the novel wearable neck brace is designed and fabricated, and its potential as a traction application device is explored.

II. MATHEMATICAL MODEL

A. Physical Structure

The mechanism (shown in Fig. 1) consists of 4 chains, an end-effector frame $\mathcal{F}_P$, and a base frame $\mathcal{F}_O$. The points S_1, Q_1, A_1 within chain 1 and points S_4, Q_4, A_4 within chain 4 are constrained to lie within the XOZ plane of the base frame. Similarly, points S_2, Q_2, A_2 within chain 2 lie on a vertical plane at $\angle S_1OS_2 = 60°$ to the X-axis. Similarly, the points S_3, Q_3, A_3 within chain 3 lie on a vertical plane at $\angle S_1OS_3 = 120°$ to the X-axis.

Each chain has a $RPUR$ structure shown in Fig. 2. S_i and E_i are revolute (R) joints, S_i and Q_i are connected by a prismatic joint (P), Q_i is a universal (U) joint consisting of two revolute joints. L, l are the heights of the end-effector and the plane containing A_i relative to the fixed base frame $\mathcal{F}_O$, respectively.

The axis of the revolute joint located at S_i and the axis of the first revolute joint located at Q_i within the universal joint in the chain are parallel. The axis of the second revolute joint within the universal joint located at Q_i and the axis of the revolute joint located at E_i intersect at a point A_i. The points

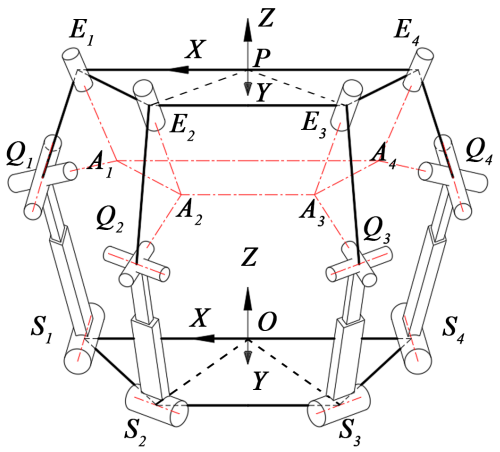

Fig. 1. Structure and math model of 2-DOF neck brace in the neutral configuration

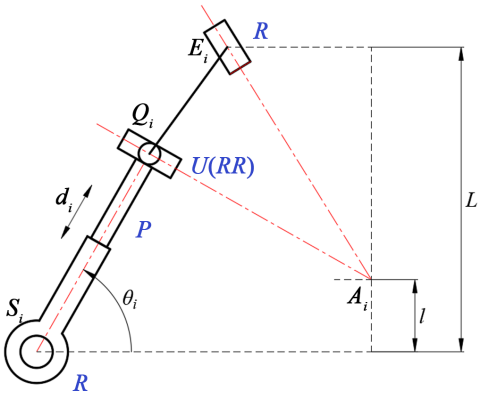

Fig. 2. Structure of each chain of 2-DOF neck brace

S_i, Q_i, and A_i are coplanar within each chain. The axis of the prismatic joint is normal to the first pair of revolute joints. The points S_1, S_2, S_3, S_4 are located on a semi-circle with a radius of r_S and sit on the fixed shoulder of the human user, considered as the fixed global frame. The intersection points A_1, A_2, A_3, A_4 are shown in Fig. 1.

In the neutral configuration, these points are chosen to lie on a circle of radius r_A that form a virtual intermediate plane that is parallel to the end-effector plane and the base plane. With this choice in the neutral configuration, the plane formed by the intersection points A_1, A_2, A_3, A_4 will remain parallel to the plane formed by the intersection points E_1, E_2, E_3, E_4. In the physical design of the mechanism, the stroke lengths of both linear actuators are 25mm.

The prismatic joints on chains 1 and 4 are actively controlled by linear actuators, while the prismatic joints on chains 2 and 3 are passive. d_1, d_4 are stroke lengths of linear actuated joints, while d_2, d_3 are stroke lengths of passive prismatic joints.

B. Description of the End-effector Motion

The three orientation angles are described in the fixed coordinate frame in Fig. 3. A space-fixed 3-1-2 angle sequence

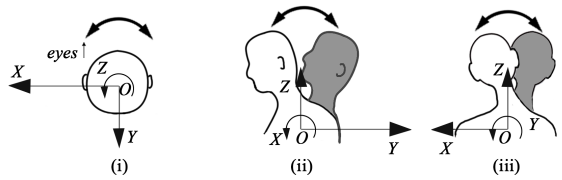

Fig. 3. Description of orientation of the head in fixed frame: (i) axial rotation α, (ii) flexion and extension β, (iii) lateral bending γ

is selected to describe the orientation of the end-effector frame $\mathcal{F}_P$ relative to the base frame $\mathcal{F}_O$. This rotation matrix is given in Eq. (1), where $\sin\beta$ is simplified as s_β, $\cos\beta$ is simplified as c_β and so on. Axial rotation, flexion/extension, and lateral bending are denoted as α, β, and γ.

$$^{O}R_P = \begin{bmatrix} s_\alpha s_\beta s_\gamma + c_\gamma c_\alpha & c_\alpha s_\beta s_\gamma - c_\gamma s_\alpha & c_\beta s_\gamma \\ s_\alpha c_\beta & c_\alpha c_\beta & -s_\beta \\ s_\alpha s_\beta c_\gamma - s_\gamma c_\alpha & c_\alpha s_\beta c_\gamma + s_\gamma s_\alpha & c_\beta c_\gamma \end{bmatrix} \quad (1)$$

The next step is to express the coordinates of E_1, ...,E_4 and $A_1, ..., A_4$ which are fixed points in the end-effector frame $\mathcal{F}_P$ in the fixed base frame $\mathcal{F}_O$, as shown in Eqs. (2) and (3). The symbols for the points in the end-effector frame $\mathcal{F}_P$ are $^{\mathcal{F}_P}E_i$ or $^{\mathcal{F}_P}A_i$, $i = 1, ..., 4$. The coordinates of these points in the base frame $\mathcal{F}_O$ are given below, where $^{\mathcal{F}_O}P$ is the coordinate of the origin which lies at the midpoint of E_1E_4 on the end-effector frame $\mathcal{F}_P$.

$$^{\mathcal{F}_O}E_i = {}^{\mathcal{F}_O}P + {}^{O}R_P\,{}^{\mathcal{F}_P}E_i, i = 1, ..., 4 \quad (2)$$

$$^{\mathcal{F}_O}A_i = {}^{\mathcal{F}_O}P + {}^{O}R_P\,{}^{\mathcal{F}_P}A_i, i = 1, ..., 4 \quad (3)$$

From the specific constraint on the geometry, A_1 and A_4 are limited to XOZ plane, i.e. the y-coordinates of these points are zero and satisfy Eqs. (4) and (5).

$$^{\mathcal{F}_O}A_{1y} = {}^{\mathcal{F}_O}P_y + s_\alpha c_\beta r_A + s_\beta(L - l) = 0 \quad (4)$$

$$^{\mathcal{F}_O}A_{4y} = {}^{\mathcal{F}_O}P_y - s_\alpha c_\beta r_A + s_\beta(L - l) = 0 \quad (5)$$

From Eqs. (4) and (5), since $r_A \neq 0$, if $c_\beta \neq 0$, the term s_α should be zero, i.e., $\alpha = 0$. In other words, the term $s_\alpha c_\beta r_A$ in Eq. (4) and $-s_\alpha c_\beta r_A$ in Eq. (5) should be zero. This implies that the axial rotation of the end-effector is zero. If $c_\beta = 0$, it implies that the lateral bending of the end-effector is $\frac{\pi}{2}$. In general, this specific pose of the end-effector, i.e., the head relative to the shoulder, with $\beta = \pi/2$, is unreachable due to geometric constraints. Thus, the rotation matrix (1) can be simplified with the condition $\alpha = 0$.

Additionally, $^{\mathcal{F}_O}P_y + s_\beta(L - l) = 0$. The geometric constraints on the locations of A_2 and A_3 create Eqs. (6) and (7):

$$^{\mathcal{F}_O}A_{2y} = \tan 60^\circ\,{}^{\mathcal{F}_O}A_{2x} \quad (6)$$

$$^{\mathcal{F}_O}A_{3y} = \tan 120^\circ\,{}^{\mathcal{F}_O}A_{3x} \quad (7)$$

From the above equations, on simplification, we get $^{\mathcal{F}_O}P_x = -\sqrt{3}/2 r_A s_\beta s_\gamma + c_\beta s_\gamma(L - l)$ and Eq. (8):

$$c_\beta = c_\gamma \quad (8)$$

According to Eq. (8), the flexion/extension motion and lateral bending are coupled together as $\beta = \gamma$ or $\beta = -\gamma$. Based on such relationship, other end-effector positions $^{\mathcal{F}_O}P_x$, $^{\mathcal{F}_O}P_y$ can then be determined with γ and $^{\mathcal{F}_O}P_z$ chosen independently.

C. Inverse Kinematics

The inverse kinematics problem is to find the displacement of each prismatic joint given the position and orientation of the end-effector. As described in the previous section, for an end-effector with 2 DOF, one can choose the following two independent variables γ, $^{\mathcal{F}_O}P_z$ to describe the position and orientation of the end-effector and the remaining end-effector position/orientation variables will be determined.

The lengths of prismatic joints can be solved by the distance equations given in Eqs. (9) and (10):

$$||^{\mathcal{F}_O}A_i - {}^{\mathcal{F}_O}Q_i||^2 = ||A_iQ_i||^2, i = 1, ..., 4 \quad (9)$$

$$||^{\mathcal{F}_O}E_i - {}^{\mathcal{F}_O}Q_i||^2 = ||E_iQ_i||^2, i = 1, ..., 4 \quad (10)$$

These distance equations will result in Eqs. (11) and (12) with the following structure:

$$f_{A_iQ_i}(d_i, \theta_i) = 0, i = 1, ..., 4 \quad (11)$$

$$f_{E_iQ_i}(d_i, \theta_i) = 0, i = 1, ..., 4 \quad (12)$$

In total, there will be 8 equations involving 8 variables as described in Eqs. (11) and (12). Solutions to these equations are resolved in scipy numerical solver of Python 3.9.

Sample Solutions: The solution sets for d_1,...,d_4 representing $S_1Q_1E_1$,...,$S_4Q_4E_4$ using Eqs. (11) and (12) for each chain were computed for an example end-effector pose: $\gamma = 5^\circ$, $^{\mathcal{F}_O}P_z = 200$ mm. For each configuration $\gamma = \beta$ and $\gamma = -\beta$, we obtained 16 real solutions of the joint variables. Each chain yielded two real solutions of the stroke length d_i, which together resulted in $2 \times 2 \times 2 \times 2 = 16$ solutions.

However, these 16 solutions are not all physically realizable as each chain can be in an 'arm up' or an 'arm down' configuration. Also, there are physical limits on the range of motion, i.e., the stroke length of each d_i. Once any chain has been assembled in an 'arm up' or an 'arm down' configuration, the stroke lengths on the chains may not be allowed to flip between the two configurations. Hence, out of the 16 potential solutions from the inverse kinematics that we obtained for $\gamma = \beta$ and $\gamma = -\beta$, we present the two solutions that are physically realizable within the structure of the neck brace assembly. Each of these two configurations is shown in a 3D geometrical model in Fig. 4. The corresponding numerical solutions are listed in Table I.

TABLE I

JOINT VARIABLES AND POSE VARIABLES IN FIG. 4 (UNIT: MM)

Sol. No.	γ	$^{\mathcal{F}_O}P_z$	β	d_1	d_4	d_2	d_3
(I)	5°	200	5°	13.70	41.02	33.67	47.54
(II)	5°	200	-5°	13.70	41.02	10.45	23.75

The first column of Table I represents the names of the solutions in Fig. 4. The second and third columns in Table

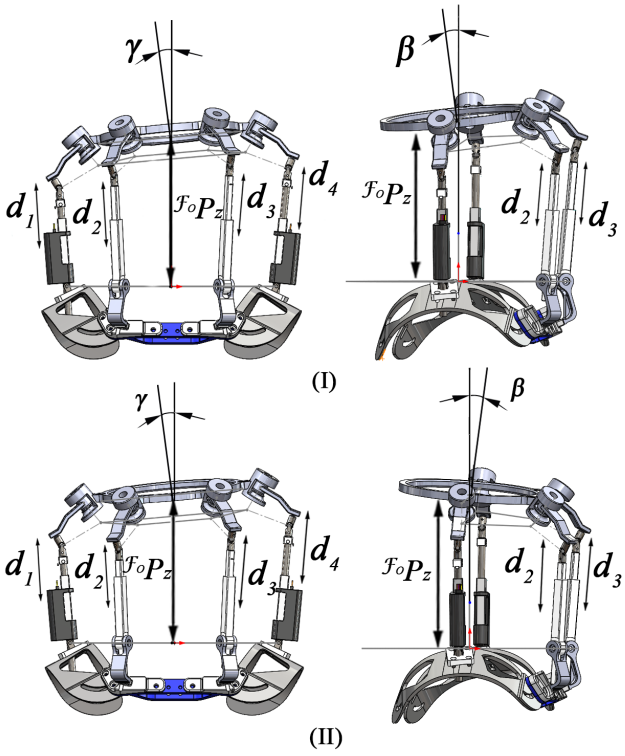

Fig. 4. Two realizable solutions of the inverse kinematics of the 2DOF neck brace

I list the end-effector pose. The last 4 columns are the solutions of the joint variables when $\beta = \gamma$ and $\beta = -\gamma$.

If the input parameter $\gamma = 0°$, there will be only 1 solution for inverse kinematics. Otherwise, for a specific input when $\gamma \neq 0°$, the computations show that there are 2 feasible solutions.

D. Forward Kinematics

Forward kinematics computes the end-effector position and orientation given the joint displacements. Here, the inputs provided are stroke lengths from chain $S_1Q_1E_1$ and chain $S_4Q_4E_4$, two equations related to ${}^{\mathcal{F}_O}P_z$ and lateral bending angle γ are:

$$f_1({}^{\mathcal{F}_O}P_x, {}^{\mathcal{F}_O}P_y, {}^{\mathcal{F}_O}P_z, \beta, \gamma, d_1) = 0 \quad (13)$$

$$f_2({}^{\mathcal{F}_O}P_x, {}^{\mathcal{F}_O}P_y, {}^{\mathcal{F}_O}P_z, \beta, \gamma, d_4) = 0 \quad (14)$$

Eqs. (13) and (14) are obtained from chain $S_1Q_1E_1$ and $S_4Q_4E_4$ and they contain the variables ${}^{\mathcal{F}_O}P_x$, ${}^{\mathcal{F}_O}P_y$, ${}^{\mathcal{F}_O}P_z$, β and γ.

In addition, we know that there are two branches of solution $\beta = \gamma$ or $\beta = -\gamma$. On substituting these (shown in Eqs. (4), (5), (6) and (7)), there remain only two independent unknowns ${}^{\mathcal{F}_O}P_z$, γ. The coupled motion of flexion/extension and lateral bending are not limitations since the traction will happen almost quasi-statically [11].

In order to verify the computations, we chose the same input stroke lengths as in Table 1, i.e., d_1 = 13.70 mm, d_4 = 41.02 mm. We found that there are four solutions when $\gamma = \beta$ and another four when $\gamma = -\beta$. Considering again the practical assembly of the solutions, we narrowed these down to two solutions which are listed in Table II and plotted in Fig. 5. These are technically the same solutions in inverse kinematics shown in Fig. 4.

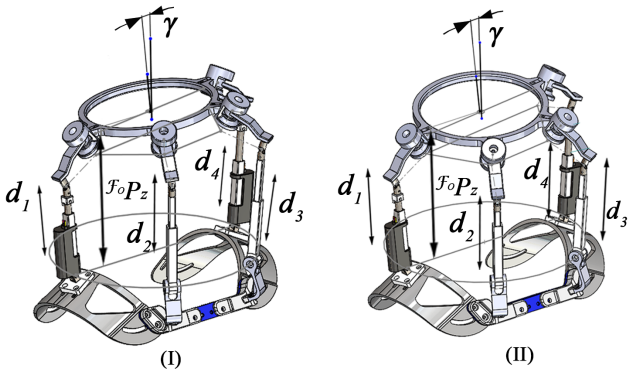

Fig. 5. Two realizable solutions of the forward kinematics of the 2DOF neck brace

The forward kinematic solutions yield the same solutions as in the inverse kinematics. This shows that the results of inverse and forward kinematics validate each other.

TABLE II
JOINT VARIABLES AND POSE VARIABLES IN FIG. 5 (UNIT: MM)

Sol. No.	d_2	d_3	γ	β	${}^{\mathcal{F}_O}P_x$	${}^{\mathcal{F}_O}P_y$	${}^{\mathcal{F}_O}P_z$
(I)	33.67	47.54	5°	5°	1.87	-2.53	200
(II)	10.45	23.75	5°	-5°	3.17	2.53	200

E. Workspace

The workspace of the mechanism is shown for two sets of parameters in Fig. 6: (i) r_A = 99.13 mm, and (ii) r_A = 20 mm. We chose r_A as a parameter to vary in the computation of feasible workspace. Other parameters that were used to compute the workspace are shown in Table III. The workspace plot in Fig. 6 shows the points where the origin of the reference frame on the end-effector can reach.

TABLE III
PARAMETERS IN TWO DIFFERENT DESIGNS (UNIT: MM)

Design	r_A	L	$L-l$	d_1	d_4
(i)	99.13	197.68	29.01	25	25
(ii)	20	197.68	29.01	25	25

In Table III, the parameter L is measured when d_1 and d_4 are at half their stroke lengths which is 25mm. This parameter is kept the same in (i) and (ii). Additionally, $L-l$ is kept the same for both designs (I) and (II). For these two different parameters, the dimension of Q_iE_i are different and results in different workspaces.

Fig. 6 shows the end-effector workspace. As r_A becomes larger, the two surfaces become more curved. A systematic study can be performed to characterize the workspace as needed in the future.

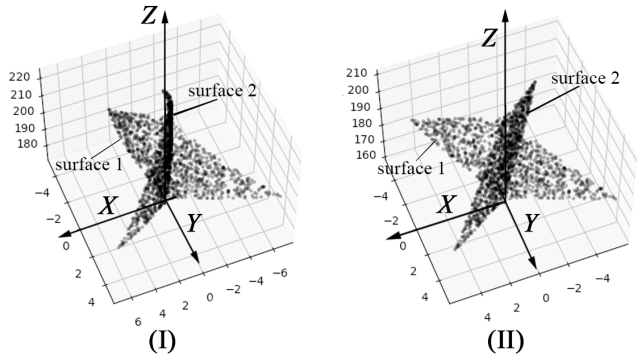

Fig. 6. Workspace of 2DOF neck brace when (I) $r_A = 99.13$mm, (II) $r_A = 20$mm, 2 surfaces in each figure contain all positions that the end-effector can reach

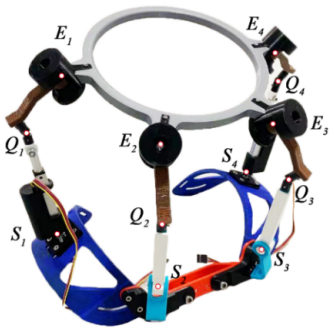

Fig. 7. Fabricated prototype of the 2DOF neck brace

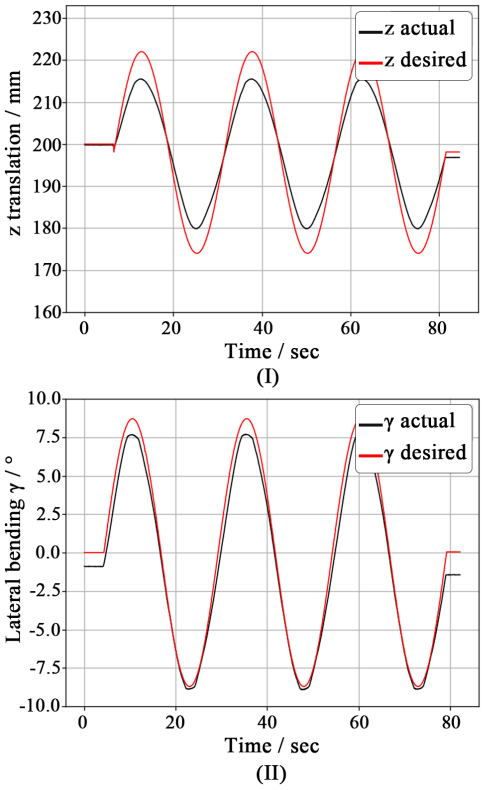

Fig. 8. (I) Z-translation and (II) lateral bending γ, validation results and desired values

III. Validation with a Prototype

In this section, a Vicon camera system is used to validate the motion of the end-effector after implementing the commands to the linear actuators.

The fabricated prototype is shown in Fig. 7 with main dimensions shown in Table IV. Except for linear actuators, universal joints, screws and bolts, all other parts were fabricated using a 3D printer. After the assembly of parts, two linear actuators were connected to a photon circuit board and were actuated. The Particle Photon has a Wi-Fi module. The linear actuators are ACTUONIX P16 Micro Linear Actuators.

The process of Vicon validation is described as 4 steps: (i) python GUI sends the commands, (ii) photon parses the commands and sends those to linear actuators, (iii) end-effector of the neck brace is driven by linear actuators, (iv) vicon cameras capture the motion of the end-effector. The tests are done with sinusoidal motion control. The sinusoidal motion is a continuous motion command to the end-effector for lateral bending and z translation. After getting the commands, the Photon controls the linear actuators to move the end-effector of the neck brace through continuous motion.

In order to know how well the system performs when following the commands, Vicon markers are placed on both the end-effector and shoulder base pad to validate the end-effector orientation and position. The motion of the end-effector is captured by Vicon Cameras and processed using Vicon Nexus software. The results from the sinusoidal motion are shown in Fig. 8.

TABLE IV
Dimensions of the Prototype (Unit: mm)

E_1E_4	S_1S_4	Q_1S_1, Q_4S_4	Q_2S_2, Q_3S_3	Q_iE_i
240	282	117.635	116.635	65.36

Table IV shows the major dimensions in the fabricated prototype. The distance S_1S_4 is selected to be twice the distance of r_S. The distance E_1E_4 is twice the distance of r_E. Distances for Q_iS_i are measured when they are not actuated. The dimension of E_1E_4 is based on the average human head size and the dimension S_1S_4 on the average size of human shoulders. Angles between Q_iS_i and plane $S_1S_2S_3S_4$ (base plane) are always larger than 90° as this is more ergonomic when participants wear the neck brace.

Fig. 8 shows the plots of the measured z-translation and lateral bending angle, distance and the commanded values. Black lines are the measured data, while the red lines are the commanded data to the mathematical model. The errors between the desired commands and the measurement from Vicon are presented in Table V.

These results show a close match between the motion of the physical prototype and the mathematical model.

TABLE V
POSITION CONTROL ERRORS

	lateral bending γ /°	z-translation ${}^{\mathcal{F}_O}P_z$ /mm
Mean Errors	0.17	3.86
RMS Errors	0.84	4.42

A. Limitations and Future Work

The differences in the features of the physical prototype and the assumptions in the mathematical model likely caused the errors observed in the position validation. Small fabrication errors, such as rotation inherent to the linear actuators, flexibility of the 3D printed links, and slight backlash in the joints can contribute to cumulative errors in the end-effector motion. Despite these unavoidable manufacturing errors, the overall motions in lateral bending and z-translation of the end-effector follow the desired motion, as shown in Fig. 8.

The current 4-chain parallel mechanism with 2-DOF of end-effector motion can provide vertical translation and lateral bending to the head-neck area. The control method in the current design is only limited to position control whereas force control is not implemented. The mechanism allows for a range of -9° to 9° lateral bending, which is adequate to automate traction provided by physical therapists. As discussed in the introduction, mechanical traction force with lateral bending, can reduce neck pain and our device can provide such a motion [10]. Human experiments will be conducted in the near future to show the viability of applying traction forces.

IV. CONCLUSIONS

The paper describes the design of a 4-chain parallel mechanism that provides 2-DOF motion to the end-effector. We motivated this mechanism to provide traction force on the head-neck along vertical direction while orienting the head to provide lateral bending. The study of this 4-chain architecture is unique and different from all previous designs of head-neck braces that allow rotation to the head-neck. We characterized its inverse and forward kinematics. We fabricated a prototype to show the physical realizability of this design and how potential manufacturing errors can impact its performance. The prototype followed the mathematical model quite well despite potential errors in fabrication. This design opens up new possibilities for use in medical applications relating to the head-neck.

ACKNOWLEDGMENT

This work was supported in part by the ALS Association under Grant 21-MALS-568, in part by the Columbia University School of Engineering seed funding through the STAR program, in part by the New York State Spinal Cord Injury Research Board (NYS SCIRB) under Institutional Grant C38336GG, in part by the NYS SCIRB Predoctoral Fellowship under Grant C39062GG.

REFERENCES

[1] H. Ahmad and H. Al-Shatoury. (2021). [Online]. Available: https://emedicine.medscape.com/article/306036-overviewa6?form=fpf

[2] W. F. LESTINI and S. W. WIESEL, "The pathogenesis of cervical spondylosis." *Clinical Orthopaedics and Related Research (1976-2007)*, vol. 239, pp. 69–93, 1989.

[3] D. L. Corey and D. Comeau, "Cervical radiculopathy," *Medical Clinics*, vol. 98, no. 4, pp. 791–799, 2014.

[4] B. I. Woods and A. S. Hilibrand, "Cervical radiculopathy," *Journal of Spinal Disorders and Techniques*, vol. 28, no. 5, pp. E251–E259, 2015.

[5] S. G. Memtsoudis, A. Hughes, Y. Ma, Y. L. Chiu, A. A. Sama, and F. P. Girardi, "Increased in-hospital complications after primary posterior versus primary anterior cervical fusion," *Clinical Orthopaedics and Related Research®*, vol. 469, pp. 649–657, 2011.

[6] R. C. Huang, F. P. Girardi, A. R. Poynton, F. P. Cammisa *et al.*, "Treatment of multilevel cervical spondylotic myeloradiculopathy with posterior decompression and fusion with lateral mass plate fixation and local bone graft," *Clinical Spine Surgery*, vol. 16, no. 2, pp. 123–129, 2003.

[7] K. R. Abi-Aad and A. Derian, "Cervical traction–statpearls–ncbi bookshelf," *StatPearls [Internet]. Treasure Island (FL)*, 2022.

[8] J. A. Cleland, J. M. Whitman, J. M. Fritz, and J. A. Palmer, "Manual physical therapy, cervical traction, and strengthening exercises in patients with cervical radiculopathy: a case series," *Journal of Orthopaedic & Sports Physical Therapy*, vol. 35, no. 12, pp. 802–811, 2005.

[9] P. Moeti and G. Marchetti, "Clinical outcome from mechanical intermittent cervical traction for the treatment of cervical radiculopathy: a case series," *Journal of Orthopaedic & Sports Physical Therapy*, vol. 31, no. 4, pp. 207–213, 2001.

[10] D. S. Creighton, D. Marsh, M. Gruca, and M. Walter, "The application of a pre-positioned upper cervical traction mobilization to patients with painful active cervical rotation impairment: A case series," *Journal of back and musculoskeletal rehabilitation*, vol. 30, no. 5, pp. 1053–1059, 2017.

[11] M. Shakoor, M. Ahmed, G. Kibria, A. Khan, M. Mian, S. Hasan, S. Nahar, and M. Hossain, "Effects of cervical traction and exercise therapy in cervical spondylosis," *Bangladesh Medical Research Council Bulletin*, vol. 28, no. 2, pp. 61–69, 2002.

[12] E. Kokkoni, Z. Liu, and K. Karydis, "Development of a soft robotic wearable device to assist infant reaching," *Journal of Engineering and Science in Medical Diagnostics and Therapy*, vol. 3, no. 2, p. 021109, 2020.

[13] H. Zhang and S. K. Agrawal, "An active neck brace controlled by a joystick to assist head motion," *IEEE Robotics and Automation Letters*, vol. 3, no. 1, pp. 37–43, 2017.

[14] H. Zhang, B.-C. Chang, and S. K. Agrawal, "Using a robotic neck brace for movement training of the head–neck," *IEEE Robotics and Automation Letters*, vol. 4, no. 2, pp. 846–853, 2019.

[15] H. Zhang, B.-C. Chang, J. Andrews, H. Mitsumoto, and S. Agrawal, "A robotic neck brace to characterize head-neck motion and muscle electromyography in subjects with amyotrophic lateral sclerosis," *Annals of clinical and translational neurology*, vol. 6, no. 9, pp. 1671–1680, 2019.

[16] M. E.-H. Ibrahem, M. S. El-Mohandes, M. T. El-Wakad, and S. A. Sami, "Design and analysis of a dynamic neck brace," in *2021 3rd Novel Intelligent and Leading Emerging Sciences Conference (NILES)*. IEEE, 2021, pp. 236–240.

[17] P. K. Lingampally and A. S. Arockia Doss, "Design, implementation, and experimental study on 3-rps parallel manipulator-based cervical collar therapy device for elderly patients suffering from cervical spine injuries," in *Handbook of Smart Materials, Technologies, and Devices: Applications of Industry 4.0*. Springer, 2022, pp. 847–869.

[18] D. Wu, L. Wang, and P. Li, "A 6-dof exoskeleton for head and neck motion assist with parallel manipulator and semg based control," in *2016 International Conference on Control, Decision and Information Technologies (CoDIT)*. IEEE, 2016, pp. 341–344.

[19] Z. Huang and Q. Li, "Type synthesis of symmetrical lower-mobility parallel mechanisms using the constraint-synthesis method," *The International Journal of Robotics Research*, vol. 22, no. 1, pp. 59–79, 2003.

[20] P. Kulkarni and S. K. Agrawal, "Design and validation of a novel robotic neck brace for cervical traction," *IEEE/ASME Transactions on Mechatronics*, 2024.